Technical Note: Testing the Connection Between Hillslope Scale Runoff Fluctuations and Streamflow Hydrographs at the Outlet of Large River Basins

Ricardo Mantilla[1], Morgan Fonley[2], and Nicolás Velasquez[3]

5   [1]Department of Civil Engineering, University of Manitoba, Winnipeg, MB, Canada
[2]Alma College, Alma, MI, USA
[3]Iowa Flood Center, University of Iowa, Iowa City, IA, USA

Correspondence to: Ricardo Mantilla (ricardo.mantilla@umanitoba.ca)

10   **Abstract.** A series of numerical experiments were conducted to test the connection between streamflow hydrographs at the outlet of large watersheds and the time-series of hillslope-scale runoff yield. We used a distributed hydrological routing model that discretizes a large watershed (~17,000 km^2) into small hillslope units (~0.1 km^2) and applied distinct surface runoff time-series to each unit that deliver the same volume of water into the river network. The numerical simulations show that distinct runoff delivery time-series at the hillslope scale result in indistinguishable streamflow hydrographs at large scales. This limitation is imposed by

15   space-time averaging of input flows into the river network that are draining the landscape. The results of the simulations presented in this paper show that under very general conditions of streamflow routing (i.e., nonlinear variable velocities in space and time), the streamflow hydrographs at the outlet of basins with Horton-Strahler (H-S) order five or above (larger than 100 km^2 in our set up) contain very little information about the temporal variability of runoff production at the hillslope scale and therefore the processes from which they originate. In addition, our results indicate that the *rate of convergence* to a common hydrograph shape

20   at larger scales (above H-S order 5) is directly proportional to how different the input signals are to each other at the hillslope scale. We conclude that the ability of a hydrological model to replicate outlet hydrographs does not imply that a correct and meaningful description of small-scale rainfall-runoff processes has been provided. Furthermore, our results provide context for other studies that demonstrate how the physics of runoff generation cannot be inferred from output signals in commonly used hydrological models.

25   **1 Introduction**

The question of how river flows will change in the presence of climatic and anthropogenic changes dominates the literature in water resources journals and research conducted around the world (Arnell & Lloyd-Hughes, 2014; Blöschl et al., 2019; Gudmundsson et al., 2021; Hirabayashi et al., 2013; Whitehead et al., 2018). Slowly evolving regional climatic changes and rapid anthropogenic modifications to the landscape will impact how watersheds deliver water to communities along the river network,

30   and recognition of this fact has fostered the development of methods and techniques to address this urgent problem (Kang et al., 2016; Kourtis & Tsihrintzis, 2021). Physics-based hydrological modeling has emerged as the preferred alternative for predicting the future of the hydrological cycle under the projected changes (Barnett et al., 2008). An example of rapid anthropogenic change in the US Midwest is the use of drainage tiling, which is effective for increasing corn yields by promoting the rapid movement of subsurface flows into rivers (Fonley et al., 2021; Schilling et al., 2019; Schilling & Helmers, 2008; Velásquez et al., 2021). This

35   raises the question of how these landscape modifications will impact the cycles of flooding and droughts in future climatic scenarios (Akter et al., 2018; Júnior et al., 2015; Peng et al., 2019). In the typical approach to this question, a land-surface model is

conceptualized, calibrated, validated, and then forced with past and future climatic inputs (rainfall, radiation, relative humidity) derived from global circulation models (Barnett et al., 2008; Condon et al., 2015; Hidalgo et al., 2009; Sadeghi Loyeh & Massah Bavani, 2021; Taye et al., 2015; Quintero et al. 2018). The underlying premise is that the hillslope-scale process equations correctly describe the water movement and partitioning into runoff and infiltration. This premise allows changing parameter values to reflect future land-surface conditions (e.g., vegetation types, deforestation, land cover, land use) along with future conditions of meteorological forcing. Nevertheless, results from Huang et al. (2017) at 12 large-scale watersheds using nine models indicate significant limitations during extreme events. Some limitations can be improved by calibration at the cost of losing representation of processes such as evapotranspiration (Ahmed et al., 2023).

The use of land-surface models relies on their validation after parameter calibration (Beven, 1989). Historically, parameters in land-surface models are adjusted (calibrated) to match streamflow hydrographs at gauged sites in the outlet of large watersheds (> 100 km^2), and a portion of the data is left to validate the hydrological model using unobserved events (Bérubé et al., 2022; Gupta et al., 2006; Refsgaard, 1997; Shen et al., 2022). Once this test has been passed, a land-surface model is deemed appropriate to explore future scenarios (Sadeghi Loyeh & Massah Bavani, 2021; Schilling et al., 2008; Whitehead et al., 2018). Other data-based techniques for streamflow prediction are not appropriate to address these questions because their parameters cannot be directly linked to physical processes and because there is a recognition that non-stationarities render historical information unreliable to predict the future behavior of hydrological systems (Bayazit, 2015; Cancelliere, 2017; Milly et al., 2008; Salas et al., 2018). Furthermore, a recent simulation based study by Remmers et al. (2020) concluded that "it is challenging and in most cases impossible to infer model structure from model output for the part of model space, bucket-based hydrological models, that [were] sampled". This raises the question, what are the mechanisms that blur such differences? In this sense, different authors have arrived at similar conclusions. According to De Boer-Euser et al. (2017), it is challenging to link hydrograph differences and model structure components. Moreover, in an intercomparison experiment of three models, Vetter et al. (2015) observed similar performance among them. Tijerina et al., (2021) described similar spatial performance of two hydrological models over the conterminous US. More recently, Mai et al. (2022) compared 13 models and obtained different orders in the best-performing models when evaluating discharge and distribution variables such as snow-water equivalent (SWE).

To investigate the validity of using land-surface models to simulate future hydrological scenarios, we explored how different hillslope scale (~ 0.1 km^2) surface runoff time-series correspond to hydrographs at the outlet of larger scales (> 100 km^2) basins. For validation, we used a distributed hydrological model that discretizes the landscape into small hillslope control volumes interconnected by the full extent of the river network of the Cedar River basin (~17,000 km^2). We created a set of forcing signals that are significantly different from each other but share the same volume of water injected into the hillslope surface. Each of the input signals represents the output of distinct land-surface process descriptions. Our results show that input signals that are very different from each other at the hillslope scale can produce streamflow hydrographs at large scales that are indistinguishable from each other. This result implies that our ability to reproduce hydrographs at the outlet of a large basin is not a reliable indicator that we have correctly described small-scale processes controlling runoff production that include the description of vegetation, soil types, land use practices, snowmelt rates, etc. Our results also provide an explanation for why it is difficult, if not imposible, to establish a causal link between runoff generation mechanisms and output hydrographs as discussed by Remmers et al., (2020).

Our paper is organized as follows: In section 2, we present the main methodological steps of our work, including the description of the routing model, the river network used, the input signals representing surface runoff, and the metrics for comparison of similarity between hydrographs. In section 3, we present the main results of the simulations for three levels of complexity in the description of flow routing. Section 4 discusses the results and how they furnish the basis for the conclusions presented in Section

80   5.

2 Methodology and Data

2.1 The Hydrological Model & The River Network

The distributed hydrological model used in this study can be succinctly described as a nonlinear water transport equation through a directed river, which is the routing component of the operational flood forecasting model HLM (Mantilla et al., 2022). The model

85   is formulated in the context of a mass conservation equation developed by Gupta and Waymire (1998), and uses the water velocity parameterization given by Mantilla (2007) where flow velocity for any link j in the river network at time t is given by $v(j, t) = v_o q_{j,n}^{\lambda_1} A_j^{\lambda_2}$, where $q_{j,n}$ is the flow from the channel link j toward the downstream channel link n, which is further related to water storage in the link $s_c^{(j)}$ by the relation $q_{j,n} = \frac{v(j,t)}{l_j} s_c^{(j)}(t)$. The equation is non-homogeneous, therefore, the velocity v_o given in $[m/s]$ is a reference quantity that corresponds to the flow velocity for a channel link that drains a $1\ km^2$ catchment when

90     $1\ m^3/s$ flows through. The parameterization replaces the momentum conservation equation (see Mantilla (2007) for details) and is equivalent to the kinematic wave simplification of the Saint-Venant equations integrated over the channel length. The parameterization is given by,

$$\frac{dq_{j,n}(t)}{dt} = \frac{v_o q_{j,n}^{\lambda_1}(t) A_j^{\lambda_2}}{l_j(1-\lambda_1)} \left(q_{p,c}(j,t) - q_{j,n}(t) + \sum_{f \to j} q_{f,j}(t) \right) \tag{1}$$

The parameters λ_1 and λ_2 represent nonlinearities introduced by changes in the link flow velocity as a function of storage in the

95   channel and on systematic changes in local and downstream hydraulic geometry, which are a function of the upstream area A $[km^2]$ and streamflow $q_{j,n}$ given in $[m^3/s]$. The index f in the equation refers to the set of upstream links draining into link j. The parameterization is equivalent to assuming that the channel slope is equal to the slope of the water surface (normal flow) and that the flow is purely kinematic, obeying a power law relation between flow depth and velocity (such as Manning, Chezy, or the Darcy-Weisbach equations). The function $q_{p,c}(j,t)$ represents the flow from the hillslope j into the channel link j. For this paper,

100   the runoff function is,

$$q_{p,c}(j,t) = q_{p,c}(j,0) + a_h^{(j)} \int_0^t p(t-\tau) e^{-k_p \tau} d\tau \tag{2}$$

where the parameter k_p is the inverse residence time in the hillslope surface when water flows at constant velocity v_h, i.e. $q_{p,c}(j,t) = a_h^{(j)} k_p s_p^{(j)} = a_h^{(j)} \left(\frac{v_h}{l_h^{(j)}} \right) s_p^{(j)}$ over the hillslope length $l_h^{(j)}$, and $p(t)$ represents the flow of water into the hillslope surface in units of $[L/T]$ (e.g., mm/hr). In hydrological models, the function $p(t)$ can represent precipitation or be the result of other

105   physical processes represented in the land-surface model that control the vertical movement of water into the hillslope surface, including interception, evaporation, infiltration, and exfiltration.

The river network chosen for this study was the Cedar River upstream of Cedar Rapids, Iowa (Figure 1). We chose this network to maintain the realism of the connectivity structure. However, simulations not presented in this paper indicate that our results can be generalized to any random-self similar network. At the outlet, the network reaches a Horton order of 8, with a width function

110   that shows the largest accumulation of channels at a common distance in the upper region of the watershed (Figure 1a). We also

show width functions for select smaller Horton-order locations in the river network to illustrate the natural variability of river network connectivity across scales.

2.2 Development of Hillslope-scale Runoff Fluctuations

In general, any rainfall pattern which is integrable over an interval of length can be written in terms of a Fourier series expansion

115   as

$$p(t) = \frac{a_0}{2} + \sum_{n=1}^{N} a_n \cos\left(\frac{2\pi nt}{T_r} - \varphi_n\right), \tag{3}$$

where phase shifts allow us to represent sines (typically present in the Fourier series expansion) in terms of cosines of the same period. In this format, the coefficients can be chosen to sufficiently represent any function, including those that are not smooth.

We applied inverted and shifted cosines representing one, two, three, and four cosine waves distributed over the course of one or

120   three days. The cosines were shifted to affirm they were nonnegative and inverted—beginning and ending with zero precipitation intensity—to impose smoothness on the rainfall signal. We included both right-skewed and left-skewed sawtooth (linear) patterns and signals depicting uniform precipitation over 1, 2, 3, and 6 days.

Input to the model was applied as flux into a hillslope surface represented by a linear reservoir that feeds into the adjacent river link. Each input waas designed to deliver 48 mm of water to the hillslope, and each signal began at time zero. Flow in the river

125   network was primed by simulating a one-day rainfall event and allowing the system to drain for ten days before applying the rainfall signal so that each link of the river network had an initial flow that was commensurate with the watershed it drained.

2.3 Developing a Reference Hydrograph for Each Location in the River Network

Comparing hydrographs across scales can be difficult due to the variability involved. To address this difficulty, we created dimensionless hydrographs for all locations in the river network with the following equations:

130   $$q^* = \frac{q}{q_{ref}} \qquad \text{and} \qquad t^* = \frac{t}{t_{ref}} \tag{4}$$

where q_{ref} is a reference maximum streamflow and t_{ref} is a reference hydrograph time to peak. For reference we chose the instantaneous unit hydrgraph that resulted from applying precipitation via a delta-Dirac function, such that the volume of water was directly applied as an initial condition onto the hillslope surface, acting as an instantaneous event. From that hydrograph, we identified the peak flow and the time to peak flow for every link in the river network. We defined an event's 'end' as the moment

135   when the flow was smaller than 1% of the peak flow.

2.4 Analysis of Convergence of Streamflow Signals at Larger Scales

To analyze the convergence of the hydrographs for streams of order ω, we compared moments about the time-axis (t^*) and about the streamflow-axis (q^*). We computed the first moment in t^* and in q^* as

$$M_1^{t^*}(\omega) = \frac{\int_0^{T^*} t^* \cdot q^*(t^*) dt^*}{\int_0^{T^*} q^*(t^*) dt^*} \tag{5}$$

140   $$M_1^{q^*}(\omega) = \frac{\int_0^{T^*} q^*(t^*) dt^*}{\int_0^{T^*} t^* dt^*}, \tag{6}$$

and the second-centered moment with the following equations,

$$M_2^{t^*}(\omega) = \frac{\int_0^{T^*} (t^* - M_1^{t^*})^2 \cdot q^*(t^*) dt^*}{\int_0^{T^*} q^*(t^*) dt^*} \tag{7}$$

$$M_2^{q^*}(\omega) = \frac{\int_0^{T^*}(q^* - M_1^{q^*})^2 dt^*}{\int_0^{T^*} t^* dt^*} \tag{8}$$

Using these definitions of moments, a ratio of the moments between two different hydrographs can be defined as

$$R_{i(A|B)}^Z(\omega_j) = \frac{max\left(M_i^Z(\omega_j)_A, M_i^Z(\omega_j)_B\right)}{min\left(M_i^Z(\omega_j)_A, M_i^Z(\omega_j)_B\right)} \tag{9}$$

where Z represents the variable of interest (in this case q^* and t^*). If the moments of two different functions, A and B, approach each other, then equation (9) tends to one in the limit as,

$$\lim_{\omega \to \infty} R_{i(A|B)}^Z(\omega) = 1 \tag{10}$$

The min and max functions in equation (8) guarantee that the limit will be reached from above in all cases. This property allowed us to define a sigmoid function to characterize the rate of convergence to the limit of ω as,

$$\hat{R}_{i(B)}^Z(\omega) = S_f \cdot \left(1 - \frac{1}{1 + e^{(\omega_i - \omega \cdot \alpha)}}\right) \tag{11}$$

where S_f is a scale factor, ω_i is the starting Horton order, and α is a parameter controlling the shape of the curve. Larger values of α indicate rapid convergence of the curve to 1 as the Horton-order of the basin increases, and conversely, small values of α indicate slower convergence to 1.

3 Results

For each of the proposed input signals, we integrated the HLM routing equations using different assumptions about the distribution of velocity in space and time, including linear routing with constant velocity in space and time, nonlinear global self-similar routing, and locally self-similar nonlinear routing (Velasquez & Mantilla, 2020). For each setup, we obtained hydrographs at all the watershed links (43,000 in total). At the smaller scales ($\omega = 2, 3,$ or 4), each signal produced a distinct hydrograph. However, the hydrographs became indistinguishable with increasing Horton order.

3.1 Comparing hydrographs at multiple scales

In Figure 2, we show the resulting hydrographs at multiple scales for input signals with a duration of 3 days. The top-left panel in Figure 2 shows the different input signals used in this experiment. We chose locations in the river network corresponding to complete order streams of orders 2 to 8 to illustrate differences in hydrograph shapes at different scales. The first set of graphs shows the hydrographs calculated under the assumption of constant flow velocity in the channels (i.e. $\lambda_1 = 0$ and $\lambda_2 = 0$) for locations with increasing Horton order. We repeated the calculation using more complex nonlinear routing assumptions. In the global self-similar case, we assumed v_0, λ_1 and λ_2 to be the same in the entire network (yellow shade panels in Figure 2), while in the local self-similar case, the same parameters are variable throughout the catchment (green shaded panels in Figure 2).

3.2 Convergence

In Figure 2, we illustrate how all the 3-day duration signals tend to converge. Moreover, we can define the convergence of two or more signals relative to any signal by comparing their moments. Figure 3 shows the average value of $R_{A|B}$ for the first (circles) and the second (triangles) moments when we compare moment ratios between the LTri3Day signal with the 3DayUniform one. In both dimensions (time and magnitude, Figures 3a and b, respectively), the value of $R_{A|B}$ tends towards one with the increase of the Horton order. In the supplemental material, we illustrate how the convergence of hydrographs occurs for all links in the network

(Figure S1). The convergence of hydrographs also holds for the more complex cases of nonlinear routing under the assumption of global and local self-similarity.

3.3 General convergence to the Instantaneous Hydrograph (Dirac simulation)

To obtain a more general idea of the convergence, we computed $R_{A|B}$ for all the input signals using the Dirac function as a reference. $R_{A|B}$ at each Horton order ω was the median value obtained for all the links of order ω. The dots in Figure 4 correspond to the computed median value of $R_{A|B}$. According to our results, each signal has a different $R_{A|B}$ for $\omega = 2$, and in all the cases, tends to converge toward 1 with increasing values of ω. Moreover, the convergence rate increases as a function of the initial differences. Signals with higher $R_{A|B}$ values at $\omega = 2$ tend to converge at a faster rate than others.

We describe the convergence rate of the median values in Figure 4 using equation (7). In the equation, we fixed the scale factor S_f to 1.3, and we took $\omega_i = 2$ as the reference Horton order. Then, using the nonlinear least squares method, we adjusted the parameter α for a set of generated hydrographs. With this approach, we obtained a good representation of the signal's convergence starting at $\omega = 2$ (continuous lines in Figure 4).

According to Figure 4, the parameter α is an index of the convergence rate for any signal. Larger values of α correspond to faster convergence rates. Moreover, we found that α depends on the order of the moment, the dimension being considered (t^* or q^*), and the streamflow routing approach. In Figure 5, we present α vs $R_{A|B}(\omega = 2)$ for each moment order, dimension, and assumptions on the variability of velocities in space and time. In all cases, α was proportional to $R_{A|B}(\omega = 2)$. This means that the more different the hydrographs are at smaller scales, the faster the convergence rate will be to the Dirac shape at larger scales. The supplemental material presents convergence for the nonlinear global and local self-similarity cases (Figures S2 and S3).

We found that the lower α values in the ratio of the second moment in time (Figure 5b) correspond to lower values of $R_{A|B}$ (Figure 4b). Additionally, higher α values occur for the ratios of the second moment in q (Figure 5d), which coincide with large $R_{A|B}$ values (Figure 4b). Also, we found that the convergence rates of the linear, nonlinear, and self-similar HLM setups are more alike in t^* than in q^*.

4 Discussion & Conclusions

Hydrologists strive to "be right for the right reasons" when modeling the hydrologic cycle, however, the datasets available to validate hydrological models are sparse and often comprise only streamflow observations at the outlets of large catchments. Typically, hydrologic modelers calibrate and validate their models using available streamflow observations. Our study sheds some new light on the limits of this strategy and provides and explanation for the difficulty in establishing a causal link between small scale runoff generation processes and hydrograph shapes at the outlets of large river basins.

The moment ratios expressed in Equation 8 show how hydrographs generated by different hillslope scale runoff signals differ from each other across Horton order scales. Our study demonstrates that differences in the hydrographs at the hillslope scale are smoothed out for larger scales. The processes controlling the convergence rate are the spatial aggregation imposed by the self-similar river network draining the landscape and the attenuation that is controlled by the flow routing equations. Simulations not shown in this paper indicate that our results hold true for any self-similar network structure. However, a systematic analysis of how different network configurations determine the rate of convergence, and if self-similarity is a necessary condition, remain to be done. Two interesting findings of our study are that *i*) the rate of convergence of hydrographs to a common shape at larger

scales is proportional to how different the input signals are at the hillslope scale, and *ii*) that the convergence is independent of the assumptions on the spatial and temporal variability of in-channel velocities imposed in the routing scheme.

Typically, validation of small-scale land-surface representations relies on the ability to reproduce streamflow hydrographs at the outlet of large catchments where historical records are available. An intermediate step in developing a site-specific hydrological
215 model is calibrating its parameters that control the rainfall-runoff transformation (e.g., infiltration rates, hydraulic conductivity, interception rates) and runoff routing through the river network (e.g., channel and floodplain friction coefficients). Our results suggest that two very different descriptions of small-scale processes (e.g., variable saturated area vs. variable infiltration rates) can lead to equivalent hydrographs at larger scales. The fact that two competing hypotheses lead to the same result hampers the possibility of determining how changes in the small-scale process will affect streamflow hydrographs in larger catchments. Our
220 analysis show that the river network connectivity leads to an averaging of the runoff produced in different locations and at different times indicating that if the right volume of runoff is applied at a given Horton-scale, the hydrographs for the network five orders or above would be indistigushible.

The generic routing schemes tested in this study give us confidence that our results can be generalized to any hydrological distributed model of any basin that explicitly includes a river network with Horton-Strahler order five or larger. This extends the
225 problem of model "equifinality" to a larger problem of "equivalent models" where distinct descriptions of hillslope scale descriptions lead to the same resulting outlet hydrograph.

5 Data and Software

Data and software for this research can be found at: https://doi.org/10.5281/zenodo.7083172

Acknowledgments

230 This work was completed with support from the Iowa Flood Center, MID-American Transportation Center (Grant number: 69A3551747107), the Iowa Highway Research Board and Iowa Department of Transportation (Contract number: TR-699). RM also acknowledges current funding from NSERC (RGPIN-2023-04724) and Manitoba Hydro.

References

Ahmed, M. I., Stadnyk, T., Pietroniro, A., Awoye, H., Bajracharya, A., Mai, J., Tolson, B. A., Shen, H., Craig, J. R., Gervais, M.,
235   Sagan, K., Wruth, S., Koenig, K., Lilhare, R., Déry, S. J., Pokorny, S., Venema, H., Muhammad, A., & Taheri, M. (2023). Learning from hydrological models' challenges: A case study from the Nelson basin model intercomparison project. *Journal of Hydrology*, *623*(March). https://doi.org/10.1016/j.jhydrol.2023.129820

Akter, T., Quevauviller, P., Eisenreich, S. J., & Vaes, G. (2018). Impacts of climate and land use changes on flood risk management for the Schijn River, Belgium. *Environmental Science and Policy*, *89*(November 2017), 163–175.
240   https://doi.org/10.1016/j.envsci.2018.07.002

Arnell, N. W., & Lloyd-Hughes, B. (2014). The global-scale impacts of climate change on water resources and flooding under new climate and socio-economic scenarios. *Climatic Change*, *122*(1–2), 127–140. https://doi.org/10.1007/s10584-013-0948-4

Barnett, T. P., Pierce, D. W., Hidalgo, H. G., Bonfils, C., Santer, B. D., Das, T., Bala, G., Wood, A. W., Nozawa, T., Mirin, A. a, Cayan, D. R., & Dettinger, M. D. (2008). Human-Induced Changes United States. *Science*, *319*(February), 1080–1083.

245 Bayazit, M. (2015). Nonstationarity of Hydrological Records and Recent Trends in Trend Analysis: A State-of-the-art Review.

Environmental Processes, *2*(3), 527–542. https://doi.org/10.1007/s40710-015-0081-7

Bérubé, S., Brissette, F., & Arsenault, R. (2022). Optimal Hydrological Model Calibration Strategy for Climate Change Impact Studies. *Journal of Hydrologic Engineering*, *27*(3), 1–13. https://doi.org/10.1061/(asce)he.1943-5584.0002148

Beven, K. (1989). Changing ideas in hydrology — The case of physically-based models. *Journal of Hydrology*, *105*(1), 157–172.
250   https://doi.org/10.1016/0022-1694(89)90101-7

Blöschl, G., Hall, J., Viglione, A., Perdigão, R. A. P., Parajka, J., Merz, B., Lun, D., Arheimer, B., Aronica, G. T., Bilibashi, A., Boháč, M., Bonacci, O., Borga, M., Čanjevac, I., Castellarin, A., Chirico, G. B., Claps, P., Frolova, N., Ganora, D., … Živković, N. (2019). Changing climate both increases and decreases European river floods. *Nature*, *573*(7772), 108–111. https://doi.org/10.1038/s41586-019-1495-6

255 Cancelliere, A. (2017). Non Stationary Analysis of Extreme Events. *Water Resources Management*, *31*(10), 3097–3110. https://doi.org/10.1007/s11269-017-1724-4

Condon, L. E., Gangopadhyay, S., & Pruitt, T. (2015). Climate change and non-stationary flood risk for the upper Truckee River basin. *Hydrology and Earth System Sciences*, *19*(1), 159–175. https://doi.org/10.5194/hess-19-159-2015

De Boer-Euser, T., Bouaziz, L., De Niel, J., Brauer, C., Dewals, B., Drogue, G., Fenicia, F., Grelier, B., Nossent, J., Pereira, F.,
260   Savenije, H., Thirel, G., & Willems, P. (2017). Looking beyond general metrics for model comparison – Lessons from an international model intercomparison study. *Hydrology and Earth System Sciences*, *21*(1), 423–440. https://doi.org/10.5194/hess-21-423-2017

Fonley, M. R., Qiu, K., Velásquez, N., Haut, N. K., & Mantilla, R. (2021). Development and Evaluation of an ODE representation of 3D subsurface tile drainage flow using the HLM flood forecasting system. *Water Resources Research*, *57*(3).
265   https://doi.org/10.1029/2020WR028177

Gudmundsson, L., Boulange, J., Do, H. X., Gosling, S. N., Grillakis, M. G., Koutroulis, A. G., Leonard, M., Liu, J., Schmied, H. M., Papadimitriou, L., Pokhrel, Y., Seneviratne, S. I., Satoh, Y., Thiery, W., Westra, S., Zhang, X., & Zhao, F. (2021). Globally observed trends in mean and extreme river flow attributed to climate change. *Science*, *371*(6534), 1159–1162. https://doi.org/10.1126/science.aba3996

270 Gupta, H. V, Beven, K. J., & Wagener, T. (2006). Model Calibration and Uncertainty Estimation. In *Encyclopedia of Hydrological Sciences*. American Cancer Society. https://doi.org/https://doi.org/10.1002/0470848944.hsa138

Hidalgo, H. G., Das, T., Dettinger, M. D., Cayan, D. R., Pierce, D. W., Barnett, T. P., Bala, G., Mirin, A., Wood, A. W., Bonfils, C., Santer, B. D., & Nozawa, T. (2009). Detection and attribution of streamflow timing changes to climate change in the Western United States. *Journal of Climate*, *22*(13), 3838–3855. https://doi.org/10.1175/2009JCLI2470.1

275 Hirabayashi, Y., Mahendran, R., Koirala, S., Konoshima, L., Yamazaki, D., Watanabe, S., Kim, H., & Kanae, S. (2013). Global flood risk under climate change. *Nature Climate Change*, *3*(9), 816–821. https://doi.org/10.1038/nclimate1911

Huang, S., Kumar, R., Flörke, M., Yang, T., Hundecha, Y., Kraft, P., Gao, C., Gelfan, A., Liersch, S., Lobanova, A., Strauch, M., van Ogtrop, F., Reinhardt, J., Haberlandt, U., & Krysanova, V. (2017). Evaluation of an ensemble of regional hydrological models in 12 large-scale river basins worldwide. *Climatic Change*, *141*(3), 381–397. https://doi.org/10.1007/s10584-016-
280   1841-8

Júnior, J. L. S., Tomasella, J., & Rodriguez, D. A. (2015). Impacts of future climatic and land cover changes on the hydrological regime of the Madeira River basin. *Climatic Change*, *129*(1–2), 117–129. https://doi.org/10.1007/s10584-015-1338-x

Kang, N., Kim, S., Kim, Y., Noh, H., Hong, S. J., & Kim, H. S. (2016). Urban drainage system improvement for climate change adaptation. *Water (Switzerland)*, *8*(7). https://doi.org/10.3390/w8070268

285 Kourtis, I. M., & Tsihrintzis, V. A. (2021). Adaptation of urban drainage networks to climate change: A review. *Science of the*

Total Environment, *771*, 145431. https://doi.org/10.1016/j.scitotenv.2021.145431

Mai, J., Shen, H., Tolson, B. A., Gaborit, É., Arsenault, R., Craig, J. R., Fortin, V., Fry, L. M., Gauch, M., Klotz, D., Kratzert, F., O'Brien, N., Princz, D. G., Rasiya Koya, S., Roy, T., Seglenieks, F., Shrestha, N. K., Temgoua, A. G. T., Vionnet, V., & Waddell, J. W. (2022). The Great Lakes Runoff Intercomparison Project Phase 4: The Great Lakes (GRIP-GL). *Hydrology and Earth System Sciences*, *26*(13), 3537–3572. https://doi.org/10.5194/hess-26-3537-2022

Mantilla, R. I., Krajewski, W. F., Velasquez, N., Small, S. J., Ayalew, T. B., Quintero, F., Jadidoleslam, N., & Fonley, M. (2022). The Hydrological Hillslope-Link Model for Space-Time Prediction of Streamflow: Insights and Applications at the Iowa Flood Center. In *Extreme Weather Forecasting*. Elsevier.

Milly, P. C. D., Betancourt, J., Falkenmark, M., Hirsch, R. M., Kundzewicz, Z. W., Lettenmaier, D. P., & Stouffer, R. J. (2008). Stationarity is dead: Whither water management? *Science*, *319*(5863), 573–574. https://doi.org/10.1126/science.1151915

Peng, Y., Wang, Q., Wang, H., Lin, Y., Song, J., Cui, T., & Fan, M. (2019). Does landscape pattern influence the intensity of drought and flood? *Ecological Indicators*, *103*(December 2017), 173–181. https://doi.org/10.1016/j.ecolind.2019.04.007

Quintero, F., Mantilla, R., Anderson, C., Claman, D., & Krajewski, W. (2018). Assessment of changes in flood frequency due to the effects of climate change: Implications for engineering design. *Hydrology*, *5*(1). https://doi.org/10.3390/hydrology5010019

Refsgaard, J. C. (1997). Parameterisation, calibration and validation of distributed hydrological models. *Journal of Hydrology*, *198*(1–4), 69–97. https://doi.org/10.1016/S0022-1694(96)03329-X

Sadeghi Loyeh, N., & Massah Bavani, A. (2021). Daily maximum runoff frequency analysis under non-stationary conditions due to climate change in the future period: Case study Ghareh Sou basin. *Journal of Water and Climate Change*, 1–20. https://doi.org/10.2166/wcc.2021.074

Salas, J. D., Obeysekera, J., & Vogel, R. M. (2018). Techniques for assessing water infrastructure for nonstationary extreme events: a review. *Hydrological Sciences Journal*, *63*(3), 325–352. https://doi.org/10.1080/02626667.2018.1426858

Schilling, K. E., Gassman, P. W., Arenas-Amado, A., Jones, C. S., & Arnold, J. (2019). Quantifying the contribution of tile drainage to basin-scale water yield using analytical and numerical models. *Science of the Total Environment*, *657*, 297–309. https://doi.org/10.1016/j.scitotenv.2018.11.340

Schilling, K. E., & Helmers, M. (2008). *Effects of subsurface drainage tiles on streamflow in Iowa agricultural watersheds : Exploratory hydrograph analysis*. *4506*(May), 4497–4506. https://doi.org/10.1002/hyp

Schilling, K. E., Jha, M. K., Zhang, Y. K., Gassman, P. W., & Wolter, C. F. (2008). Impact of land use and land cover change on the water balance of a large agricultural watershed: Historical effects and future directions. *Water Resources Research*, *45*(7), 1–12. https://doi.org/10.1029/2007WR006644

Shen, H., Tolson, B. A., & Mai, J. (2022). Time to Update the Split-Sample Approach in Hydrological Model Calibration. *Water Resources Research*, *58*(3), 1–26. https://doi.org/10.1029/2021WR031523

Taye, M. T., Willems, P., & Block, P. (2015). Implications of climate change on hydrological extremes in the Blue Nile basin: A review. *Journal of Hydrology: Regional Studies*, *4*, 280–293. https://doi.org/10.1016/j.ejrh.2015.07.001

Tijerina, D., Condon, L., FitzGerald, K., Dugger, A., O'Neill, M. M., Sampson, K., Gochis, D., & Maxwell, R. (2021). Continental Hydrologic Intercomparison Project, Phase 1: A Large-Scale Hydrologic Model Comparison Over the Continental United States. *Water Resources Research*, *57*(7), 1–27. https://doi.org/10.1029/2020WR028931

Velasquez, N., & Mantilla, R. (2020). Limits of predictability of a global self-similar routing model in a local self-similar environment. *Atmosphere*, *11*(8). https://doi.org/10.3390/atmos11080791

Velásquez, N., Mantilla, R., Krajewski, W., Fonley, M., & Quintero, F. (2021). Improving Hillslope Link Model Performance

from Non-Linear Representation of Natural and Artificially Drained Subsurface Flows. *Hydrology*, *8*(4), 187.

Vetter, T., Huang, S., Aich, V., Yang, T., Wang, X., Krysanova, V., & Hattermann, F. (2015). Multi-model climate impact assessment and intercomparison for three large-scale river basins on three continents. *Earth System Dynamics*, *6*(1), 17–43. https://doi.org/10.5194/esd-6-17-2015

330   Whitehead, P. G., Jin, L., Macadam, I., Janes, T., Sarkar, S., Rodda, H. J. E., Sinha, R., & Nicholls, R. J. (2018). Modelling impacts of climate change and socio-economic change on the Ganga, Brahmaputra, Meghna, Hooghly and Mahanadi river systems in India and Bangladesh. *Science of the Total Environment*, *636*, 1362–1372. https://doi.org/10.1016/j.scitotenv.2018.04.362
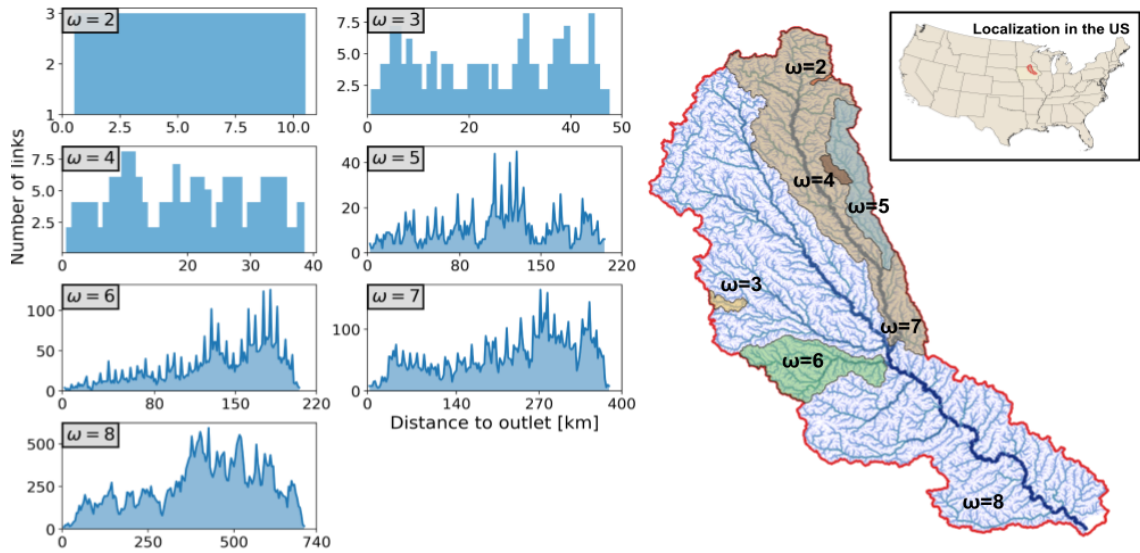
335

Figure 1. Cedar River watershed network structure (right) with the width function at the outlet ($\varpi = 8$) and at nested sub-watersheds with orders $\varpi = 2$ to 7.
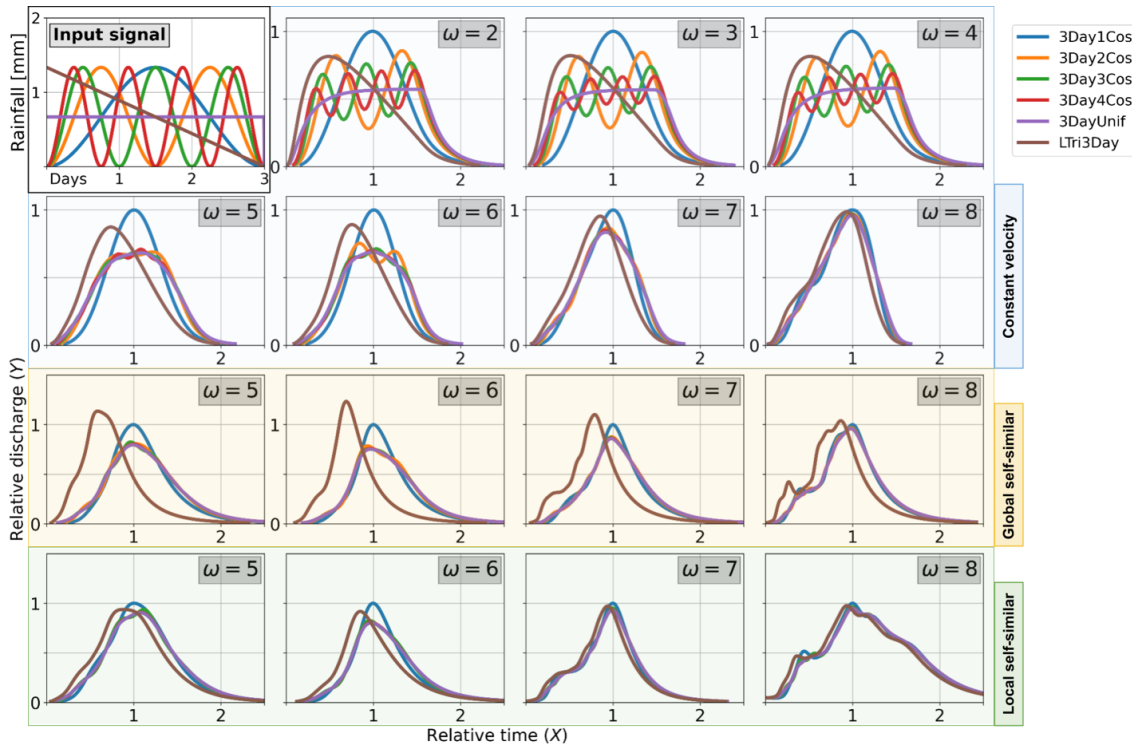
340   **Figure 2. Three-day duration input signals and resulting hydrographs at subwatersheds of orders between 2 and 8. The magnitude and time duration of the hydrographs is standardized relative to the 3Day1Cos (blue) hydrograph.**
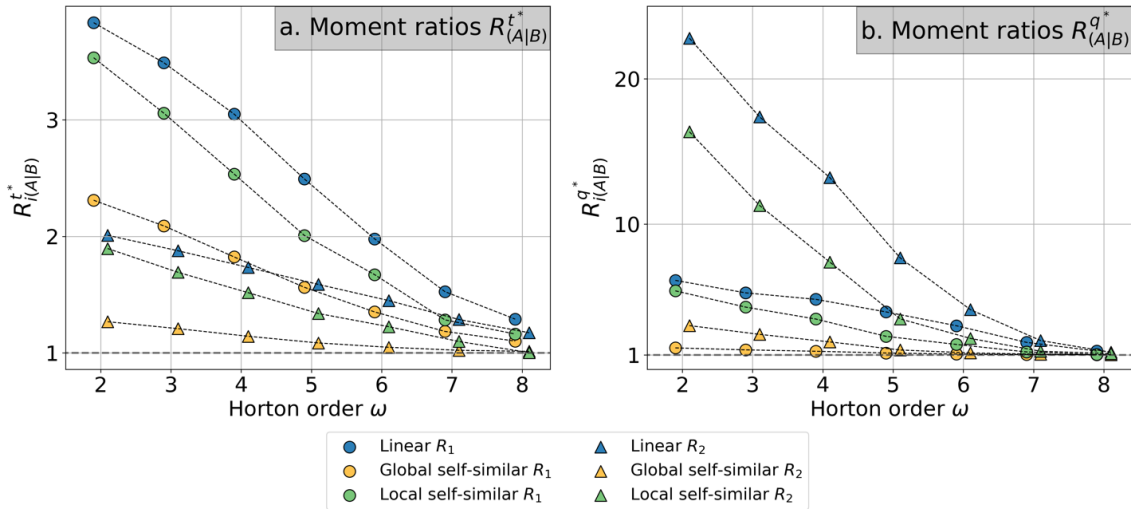
Figure 3. Changes of the first (circles) and second (triangles) moment ratios of the LTri3Day signal with respect to the 3DayUniform signal for different routing schemes. In panel a) moment ratios about the relative time $R_{i(B)}^{t^*}$, and in panel b) moment ratios about the relative streamflow $R_{i(B)}^{q^*}$.
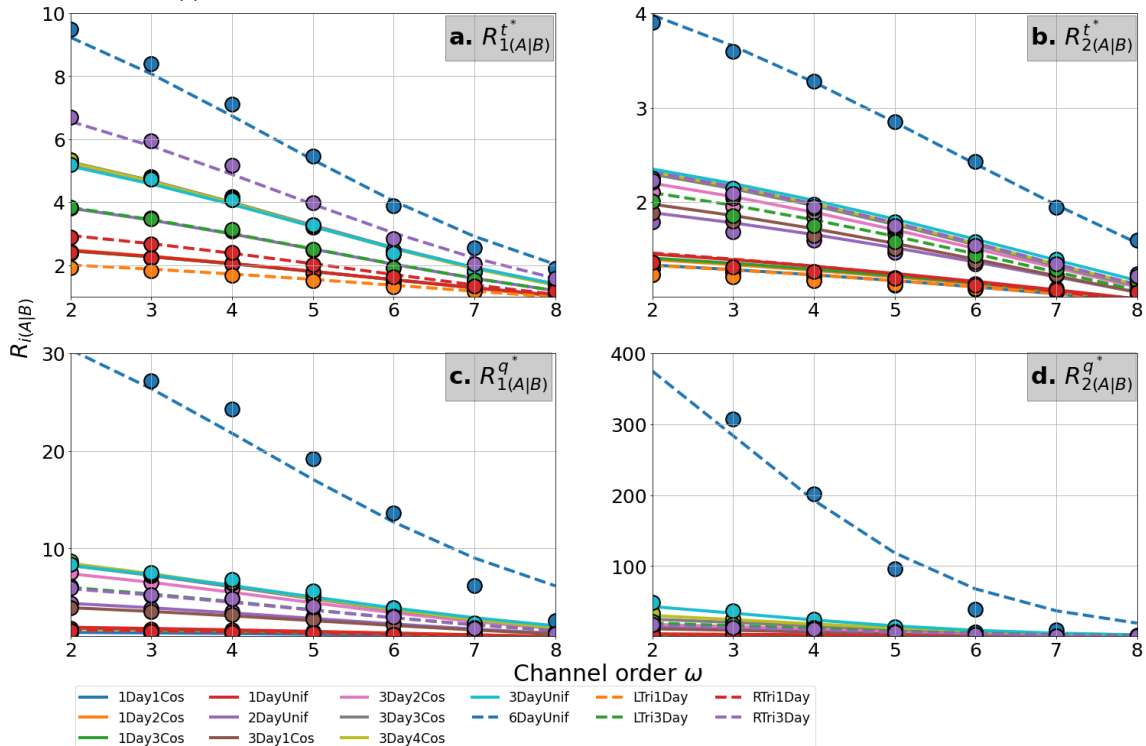
Figure 4. Convergence for all the signals relative to the Dirac assuming constant velocity routing. The dots correspond to the median value of the moments ratio R, and the lines correspond to equation (7) results.
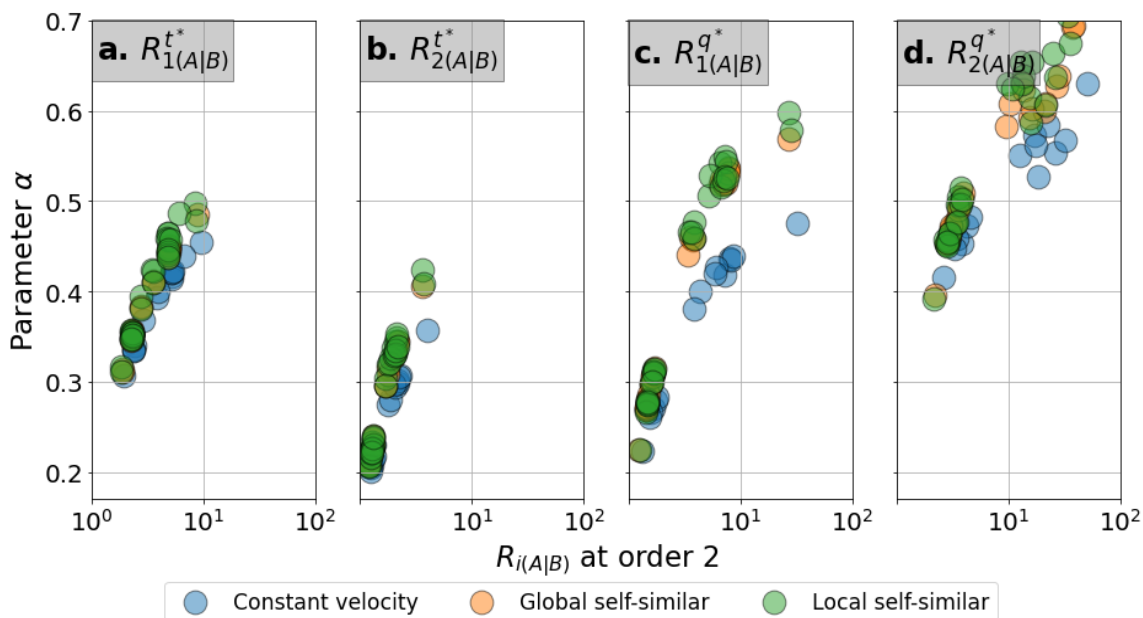
350

Figure 5. Values of the estimated parameter α as a function of moment ratios for hydographs at order 2 streams for different scenarios of routing.